

Article

Generation and Dynamics of Multiple Pulses in an Ultrafast Fiber Laser with a Single-Mode Fiber–Graded-Index Multimode Fiber–Single-Mode Fiber-Based Saturable Absorber

Yatao Yang, Qiong Zeng, Yanzhao Yang, Geguo Du, Jianhua Ji, Yufeng Song , Zhenhong Wang and Ke Wang *

College of Electronics and Information Engineering, Shenzhen University, Shenzhen 518060, China;

yatao86@szu.edu.cn (Y.Y.); 2110436132@email.szu.edu.cn (Q.Z.); yyz@szu.edu.cn (Y.Y.);

dugegu@szu.edu.cn (G.D.); jjh@szu.edu.cn (J.J.); yfsong@szu.edu.cn (Y.S.); wangzhenhong@szu.edu.cn (Z.W.)

* Correspondence: wong@szu.edu.cn

Abstract: In this study, we have investigated the evolution process and dynamic characteristics of a multi-pulse regime in an erbium-doped fiber ring laser based on a single-mode fiber–graded-index multimode fiber–single-mode fiber (SMF-GIMF-SMF) structure as an optical modulator. By utilizing the excellent nonlinear optical absorption of the SMF-GIMF-SMF (SMS) device with a modulation depth of ~8.68%, stable single-pulse mode locking at the frequency of 9.84 MHz can be readily observed at low pump power. In addition, the single-pulse operation can evolve into a multiple-pulse regime on account of the peak-power-clamping effect via suitably raising the pump power and carefully regulating the polarization state. Further, the single-shot temporal evolution of multiple pulses is monitored, indicating that this state shows unique and interesting temporal characteristics with variable pulse separations and inconsistent pulse intensities, which, as far as we know, is the first such observation in ultrafast fiber lasers. Additionally, this study, based on the time-stretch dispersive Fourier transformation method, suggests that these multiple pulses consist of chaotic wave envelopes with erratic intensities and changeable pulse energy. We believe that these findings have profound implications for revealing fascinating nonlinear pulse dynamics in ultrafast fiber optics.



Citation: Yang, Y.; Zeng, Q.; Yang, Y.; Du, G.; Ji, J.; Song, Y.; Wang, Z.; Wang, K. Generation and Dynamics of Multiple Pulses in an Ultrafast Fiber Laser with a Single-Mode Fiber–Graded-Index Multimode Fiber–Single-Mode Fiber-Based Saturable Absorber. *Photonics* **2024**, *11*, 52. <https://doi.org/10.3390/photonics11010052>

Received: 26 October 2023

Revised: 19 December 2023

Accepted: 3 January 2024

Published: 4 January 2024



Copyright: © 2024 by the authors. Licensee MDPI, Basel, Switzerland. This article is an open access article distributed under the terms and conditions of the Creative Commons Attribution (CC BY) license (<https://creativecommons.org/licenses/by/4.0/>).

Keywords: fiber laser; SMF-GIMF-SMF; mode locking; multiple pulses; dispersive Fourier transformation

1. Introduction

Lately, ultrafast fiber lasers have attracted much curiosity owing to their many potential applications in a variety of industries, including national defense [1], optical communication [2–4], precision machining [5], optical fiber sensors [6], microscopic imaging [7] and biomedicine [8]. The passive mode-locking technique is one of the most common ways to produce ultrafast pulses. When it comes to realizing the stable mode-locking pulse regime in fiber lasers, saturable absorbers (SAs) are fundamental and critical components. At present, various SAs are widely used in ultrafast fiber lasers, such as CNTs [9], graphene [10], black phosphorus (BP) [11], nonlinear polarization rotation (NPR), WS₂ [12], topological insulators (TIs) [13], semiconductor saturable absorber mirrors (SESAM) [14], transition metal dichalcogenides (TMDs) [15] and MXene [16], promoting the quick and robust development of fiber lasers. However, the NPR technique is sensitive to environmental vibration and polarization, which may lead to poor stability. In addition, these material-based SAs (graphene or black phosphorus, for instance) can show lower damage thresholds, which can ultimately result in a small power output and hinder their further application. Thus, it is of great necessity to explore SAs based on new materials or structures to overcome the deficiencies of the present SAs.

As a recent novel SA, SMS structures have the advantages of a simple process, convenient construction, good resistance to environmental interference and excellent nonlinear optical absorption at a wide band. Therefore, they have been a widespread concern both at

home and abroad. In 2013, Nazemosadat et al. proposed to exploit SMS structures that can be employed for an SA in all-fiber mode-locking fiber lasers and numerically conducted an analysis of the nonlinear multimode interference (NL-MMI) effect in SMS devices [17], verifying that GIMF possesses excellent saturable absorption properties. In addition, some researchers excavated several novel SMS devices to achieve varied mode-locked pulses. For instance, Teğın et al. proposed utilizing an SMF-SIMF-GIMF-SMF scheme in a ytterbium-doped fiber laser and obtained dissipative soliton pulses [18]. Subsequently, stable optical pulses were obtained in erbium-doped and thulium-doped fiber lasers with no core fiber (NCF)-GIMF SAs [19,20]. Recently, a tapered GIMF-based modulator has been employed to realize tunable mode-locked pulses in a thulium-doped fiber laser [21]. In 2021, an innovative hybrid structure composed of GIMF and graphene for stable optical pulses was reported by Li X et al. [22]. Moreover, some fascinating mode-locking phenomena in SMS-based mode-locked fiber lasers were observed, such as noise-like pulses [23], Q-switched mode-locking patterns [24], different bound solitons [20,25] and multi-wavelength mode-locking patterns [26]. These experimental results profoundly facilitate the development and application of GIMFs as SAs in ultrafast fiber lasers.

Apart from the generation of ultrashort pulses with broadband spectra, ultrafast fiber lasers can be used as an excellent method for investigating pulse dynamics. In addition, the fiber-like structured waveguide lasers can be used for exploring the pulse dynamics, including the pulse transition from passive Q-switching to continuous-wave mode locking [27], GHz-level mode locking [28], and single- and dual-channel Q-switching [29]. These diverse pulse evolutions can provide a broad research field for studying the characteristics and behaviors of ultrashort pulses. Further, fiber lasers with anomalous dispersion are prone to generating multiple pulses at high pump powers when there are energy quantization effects or an accumulation of excessive pulse chirps in the laser cavity. Different interactions among these multiple soliton pulses can reorganize or bind the positions, which can eventually form harmonic mode locking [30] or bound solitons [31]. The interaction forces among soliton pulses with larger intervals are weaker, forming a more unstable regime, which may contain complex pulse dynamic evolutions. In addition to their fundamental physical significance, multiple soliton pulses can be used as an alternative optical source for multilevel encoding [32], micromachining [33] and optical coherence tomography [34]. Consequently, it would be of great value to explore the dynamics and process of multiple pulses, further optimizing the design and development of ultrafast fiber lasers.

2. Fabrication and Principle

Multimode fibers with a large core diameter allow multiple spatial modes to be transmitted, and the phase velocities of the optical wave modes are not the same in different transmission modes. Therefore, when light travels in a multimode fiber, higher-order modes are excited, creating different interference fields at different locations in the multimode fiber. When a standard single-mode laser beam is injected into the GIMF, its transmission in the GIMF in a periodic interference mode can form a stable nonlinear multimode interference (NL-MMI), sometimes referred to as the self-imaging effect [35,36]. The higher-order modes are periodically interfered with and superimposed at different locations to produce different light energy distributions. The high-intensity light is gathered together and re-entered into the single-mode fiber core, which oscillates periodically in the laser cavity and finally produces a pulsed output [37].

As the degree of GIMF bending increases, the number of excited higher-order modes changes correspondingly. Meanwhile, the output beam of the multimode fiber after continuous bending undergoes periodic oscillatory coupling between the fundamental mode and the initial excited guide mode along the length direction with an equal oscillation period and interference length [38,39]. In the SMS structure, the interference length caused by the GIMF is generally in the order of 100 μm [40–42]. In order to obtain good mode-locking laser performance, it is necessary to adjust the length of the GIMF to the order of microns to achieve the best saturable absorption, which is very inconvenient for practical operation.

Theoretically, the saturable absorption mechanism in an SMS device is based on the transmission characteristics and nonlinear optical effects of optical signals in the multimode fiber [17,43]. When a low-power signal enters the multimode fiber, due to its larger mode area and multiple transmission modes, the light signal propagates through multiple paths and undergoes radiation in the cladding of the fiber. This radiation process quickly attenuates and absorbs the energy of the low-power signal, achieving a saturable absorption effect. On the contrary, high-power signals can take advantage of the larger mode area and higher transmittance of the multimode fiber, enabling them to be transmitted over longer distances with lower losses. Consequently, as the light signal passes through the SMS device, it achieves the attenuation of low-power signals and the effective transmission of high-power signals. As the light signal undergoes multiple cycles within the resonant cavity, high-energy signals gradually accumulate and interfere, ultimately achieving pulse output. The schematic diagram of the SMS-SA is shown in Figure 1a. We used a fiber fusion splicer (Fujikura 80s) to splice two segments of standard SMFs to both ends of a GIMF with a core diameter of 62.5 μm. Then, the length of the GIMF was measured to be 32.8 cm. During the fiber fusion process, the fusion mode was set as multimode-to-multimode to ensure the transmission mode matched between fibers, making fiber alignment easier and reducing optical loss. Both the SMF and GIMF are relatively cheap and can be connected using a fusion splicer, indicating that the production cost of this SA is low, and the manufacturing process is simple.

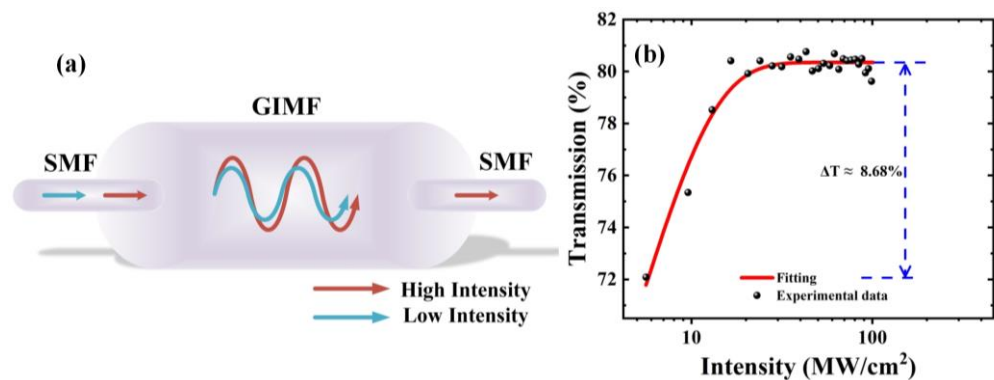


Figure 1. (a) Schematic diagram of the SMS-SA; (b) the nonlinear absorption curve of SA with SMF-GIMF-SMF structure: the black dots correspond to the experimental data, and the red line is a curve fitted by Equation (1).

To further investigate the nonlinear saturable absorption properties of the SMS-SA, we employed the balanced two-arm test method [42] to attain its nonlinear transmission curve. The curves can help evaluate the performance of the device and facilitate further optimization. The ultrashort pulse source used in the balanced two-arm test method is a home-made mode-locked fiber laser with a center wavelength of ~1561.5 nm, a spectral width of ~5.6 nm, a pulse width of 456 fs and a rate of 15.3 MHz. The nonlinear transmission curve of the fabricated SMS-SA is shown in Figure 1b, and its typical curve characteristics can be fitted by the following equation:

$$T(I) = 1 - \Delta T \times \exp\left(-\frac{I}{I_{sat}}\right) - T_{ns} \quad (1)$$

where $T(I)$ is the transmittance, ΔT is the modulation depth, I is the input light intensity, I_{sat} is the saturation fluence and T_{ns} is the nonsaturable loss. Through fitting, we obtained the saturation fluence and nonsaturable loss of the SMS device of 5.12 MW/cm² (~2.33 μJ/cm²) and 19.65%, respectively, and the measured modulation depth is ~8.68%. The experimental results demonstrate that the SMS component exhibits excellent nonlinear absorption characteristics, making it suitable for achieving ultrafast pulse output in passive mode-locked fiber lasers.

3. Experimental Configuration

To take advantage of the nonlinear absorption of the SMS structure device, a passively erbium-doped fiber (EDF) laser with an SMS-based modulator was designed. The experimental apparatus is displayed in Figure 2. The pump light operating at 980 nm was delivered into the laser cavity via a 980/1550 nm wavelength division multiplexer (WDM). A highly erbium-doped fiber (LIEKKI Er 80-8/125) of 34 cm in length with the dispersion coefficient of $-20 \text{ ps}^2/\text{km}$ @1550 nm was applied as the gain medium. The laser output was controlled by a 30% port of the optical coupler (OC). In addition, we changed the intracavity polarization state and optimized the mode-locked operation via tuning a three-paddle polarization controller (PC). The one-way laser signal transmission in the cavity can be ensured by a polarization-insensitive optical isolator (PI-ISO). The 32.8 cm GIMF (which keeps straight in the cavity) spliced with SMFs served as the mode-locked device, which was placed between the WDM and PI-ISO. The total cavity length was about 20.34 m. Except for EDF and GIMF, other fibers were standard SMFs with the dispersion coefficient of $-23 \text{ ps}^2/\text{km}$ @1550 nm. Therefore, the net cavity dispersion was anomalous. Then, the output pulse performance was evaluated by utilizing an optical spectrum analyzer (AQ6370D, Yokogawa, Tokyo, Japan), a 1 GHz oscilloscope (DSOS104A, Keysight, Santa Rosa, CA, USA), a radio-frequency (RF) spectrum analyzer (N9322C, Keysight, Santa Rosa, CA, USA) and an optical autocorrelator (FR-103XL, Femtochrome, Berkeley, CA, USA). Simultaneously, a real-time oscilloscope (DPO72004C, Tektronix, Beaverton, CA, USA) with a high-speed photodetector (New Focus Model 1444, Newport, Irvine, CA, USA) were employed to observe the internal details of the output pulses.

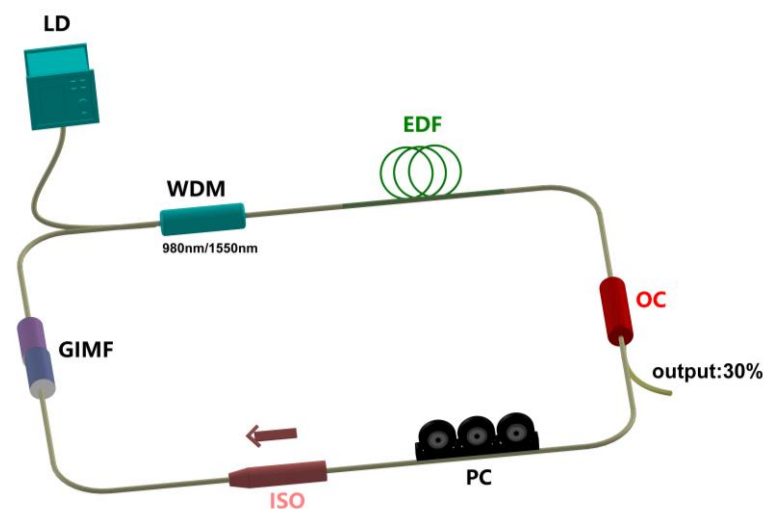


Figure 2. The schematic of the fiber laser. LD: laser diode; WDM: wavelength division multiplexer; EDF: erbium-doped fiber; OC: optical coupler; PC: polarization controller; ISO: polarization-insensitive optical isolator; GIMF: graded-index multimode fiber.

4. Experiments and Results

In this experiment, by gradually increasing pump power, the fiber laser with SMS SA can generate mode-locking pulses. When the pump power surpasses 50 mW, it is simple to obtain a stable mode locking regime by properly rotating the PC paddles. Figure 3 presents the output pulse characteristics at 55.5 mW pump power. The optical spectrum can be shown in Figure 3a with a center wavelength of $\sim 1560.50 \text{ nm}$ and spectral width of $\sim 4.98 \text{ nm}$. Additionally, the obvious Kelly sidebands are visible on both sides of the spectrum, proving that the fiber laser is operating in the anomalous dispersion region. The measured pulse trains based on the low-speed oscilloscope with 1 GHz bandwidth are displayed in Figure 3b. The repetition frequency of $\sim 9.84 \text{ MHz}$ corresponding to the temporal interval between neighboring pulses in the figure is approximately 101.6 ns, which matches the cavity length. According to the RF spectrum shown in Figure 3c, the

peak of the repetition rate is located around 9.84 MHz. With a resolution bandwidth of 100 Hz, the signal-to-noise ratio (SNR) is approximately 49 dB. This indicates a significant difference between the peak of the mode-locked signal and the background noise, which further proves that the fundamental mode-locked regime has relatively good reliability and stability. Moreover, as shown in Figure 3d, the shot-to-shot spectrum over 3000 consecutive roundtrips based on the DFT method is explored. It can be shown from the plot that the optical spectra are nearly indistinguishable from one another. In addition, the intensities at consecutive roundtrips are unchanged and no significant fluctuation is observed on the spectra, further suggesting the stable operation of the mode-locking pulses.

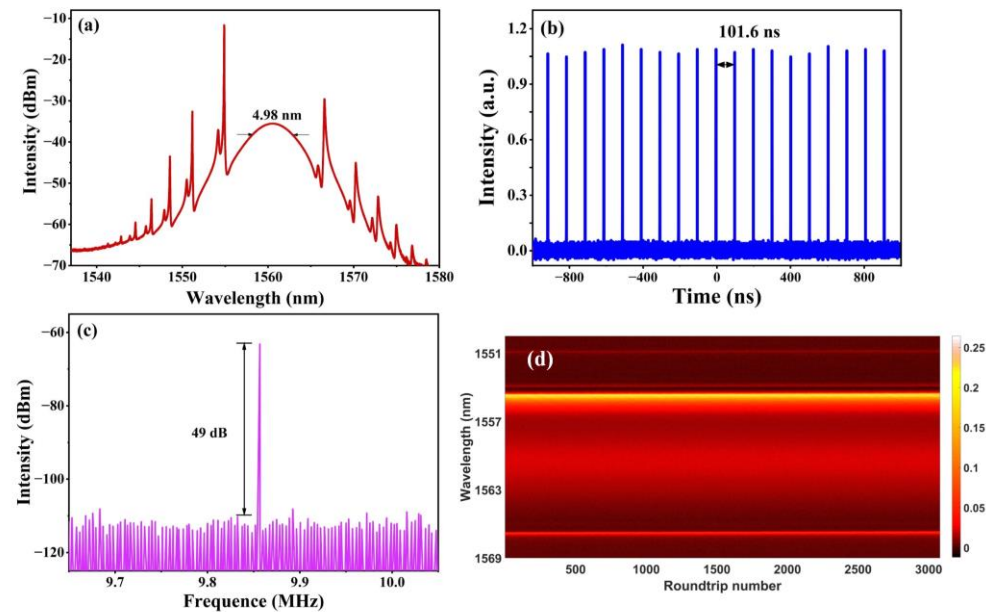


Figure 3. Output pulse characteristics of stable mode locking with a pump power of 55.5 mW. (a) Optical spectrum; (b) oscilloscope trace; (c) RF spectrum; (d) shot-to-shot spectra.

Further, by slowly raising the pump power and finely tuning the angle of the PC blades, a notable mode-locked state can be achieved. Figure 4 displays the corresponding pulse behaviors at 215 mW. The optical spectrum centers at 1558.6 nm and the measuring spectral width is 3.31 nm, as depicted in Figure 4a. As the nonlinear absorption properties of the SMS structure vary with pump powers, the spectral width of Figure 4a is narrower than that of Figure 3a when pump power increases from 55.5 mW to 215 mW. Kelly sidebands with low intensities are observed on the spectrum. Figure 4b shows the measured pulse trains by using the low-speed oscilloscope with 1 GHz bandwidth, which demonstrates that the temporal period (~ 101.6 ns) is unchanged. The RF spectrum in Figure 4c exhibits a SNR of 58 dB, with a resolution bandwidth of 100 Hz. The corresponding autocorrelation curve is present in Figure 4d. The pulse duration with the sech^2 fitting is ~ 0.727 ps, matching the full width at half maximum (FWHM) of 1.123 ps. The base intensity can result from the high gain of the autocorrelator setting.

In addition, as shown in Figure 5a, two-dimensional temporal evolution with over 3000 roundtrips is investigated. Clearly, the mode-locking regime actually consists of multiple pulses with unequal intervals. This is mainly due to the pulse energy quantization effect at higher pump power [44], resulting in the single pulses easily splitting into a lot of small pulses. In the meantime, the minimum pulse-to-pulse spacing is ~ 110 ps and the maximum one is ~ 1.16 ns, showing that the temporal separation is randomly assigned. This condition also indicates that there are relatively weak interactions existing among these multiple pulses. Moreover, the mode-locking operation still exists even when the pump power is raised. Figure 5b depicts the temporal evolution process at 415 mW pump power. In comparison to Figure 5a, it can be observed from the figure that more

multiple pulses were generated, and the locations and temporal intervals of these pulses also changed. Multiple pulses on the left are tightly distributed and those on the right are loosely distributed.

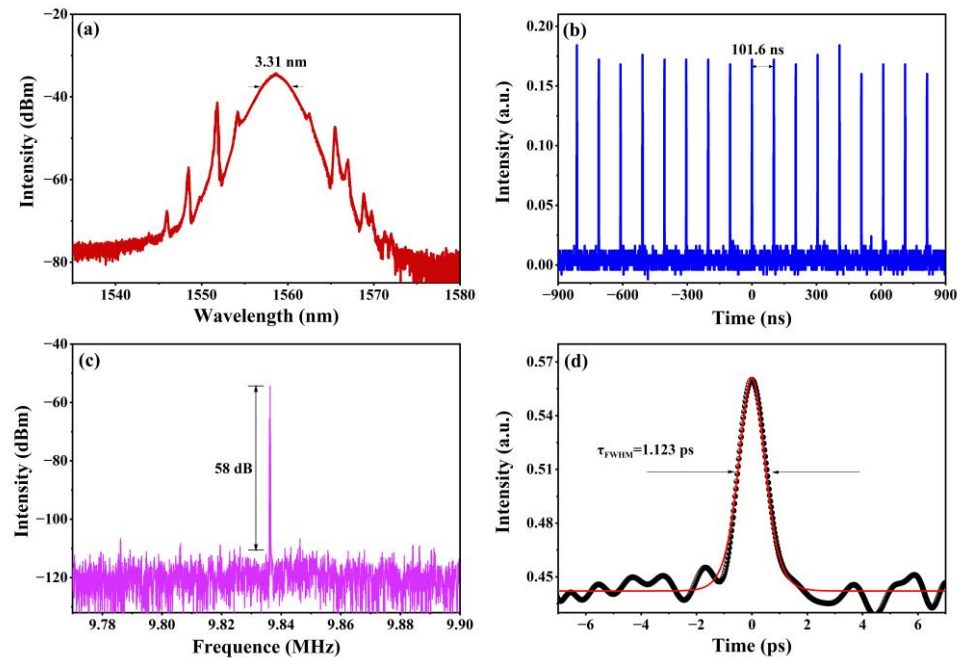


Figure 4. Output pulse characteristics of special mode locking with a pump power of 215 mW. (a) Optical spectrum; (b) oscilloscope trace; (c) RF spectrum; (d) autocorrelation trace.

To explore the real-time spectral evolution, the shot-to-shot spectra were measured for more than 3000 consecutive roundtrips using the DFT technique. The results at pump powers of 215 mW and 415 mW are shown in Figure 6a,b, where the blue curve represents the energy evolution at different roundtrips. The energy curve exhibits an unstable and non-periodic evolution. The spectral intensity and spectral width increase with increasing pumping power, and the energy curve at high power shows a more intense evolution process over the roundtrip cycles. The shot-to-shot spectrum shows that the intensity of multiple pulses is higher in the middle, and the lower spectral intensity on both sides corresponds to the Kelly sideband of the commercial spectrum. Compared with Figure 6a, Figure 6b exhibits higher spectral intensity, and the fluctuations of soliton pulses demonstrate pronounced wave-like characteristics, generating irregular pulse shapes. This phenomenon indicates that high-power soliton dynamics are more intense and disordered, likely involving complex interactions between nonlinear effects and dispersion. Investigating the soliton dynamics process at high power levels will contribute to a deeper understanding of pulse behaviors in a nonlinear medium. As illustrated in Figure 7a, the spectra of these multiple pulses at various powers are recorded. With increased pump power, the spectral bandwidth and intensity vary, and there is a clear Kelly sideband on both sides of the spectrum, while there is no significant change in the spectral shape, indicating that the cavity is in a negative dispersion state. As the pump power rises, there is a mildly blue shift in the center wavelength, showing that the cavity loss increases at high power. In this study, we observed different operating regimes by increasing the pump power. Figure 7b illustrates the operating regime distribution of the laser, along with the corresponding output power, and average pulse energy versus the pump power. The laser requires a pump power of 25 mW to achieve continuous wave output. At a pump power of 55.5 mW, we observed a single pulse mode-locking state, as shown in Figure 3. By further increasing the power and fine-tuning the PC, a stable multiple pulse mode-locking state was observed at 165 mW pump power. Interestingly, though we gradually increased the pump power to 665 mW without adjusting the PC, the special multi-pulse operation did

not have significant changes. It can be seen from Figure 7b that the average output power climbs from 6.01 mW to 32.4 mW as the pump power rises from 165 mW to 665 mW in the multiple-pulse operation. It is difficult to precisely calculate the pulse energy of the special multiple pulse operation state because there are multiple pulses with varying pulse numbers, peak power and pulse width [45,46]. However, we can estimate the pulse energy of multi-pulses by dividing the average output power by the repetition frequency [47,48]. Based on this calculation, the total pulse energy of multi-pulses increased from 0.61 nJ to 3.29 nJ versus the pump power increasing from 165 mW to 665 mW. These results are useful for researchers looking deeper into the soliton dynamics of high-average-energy pulses.

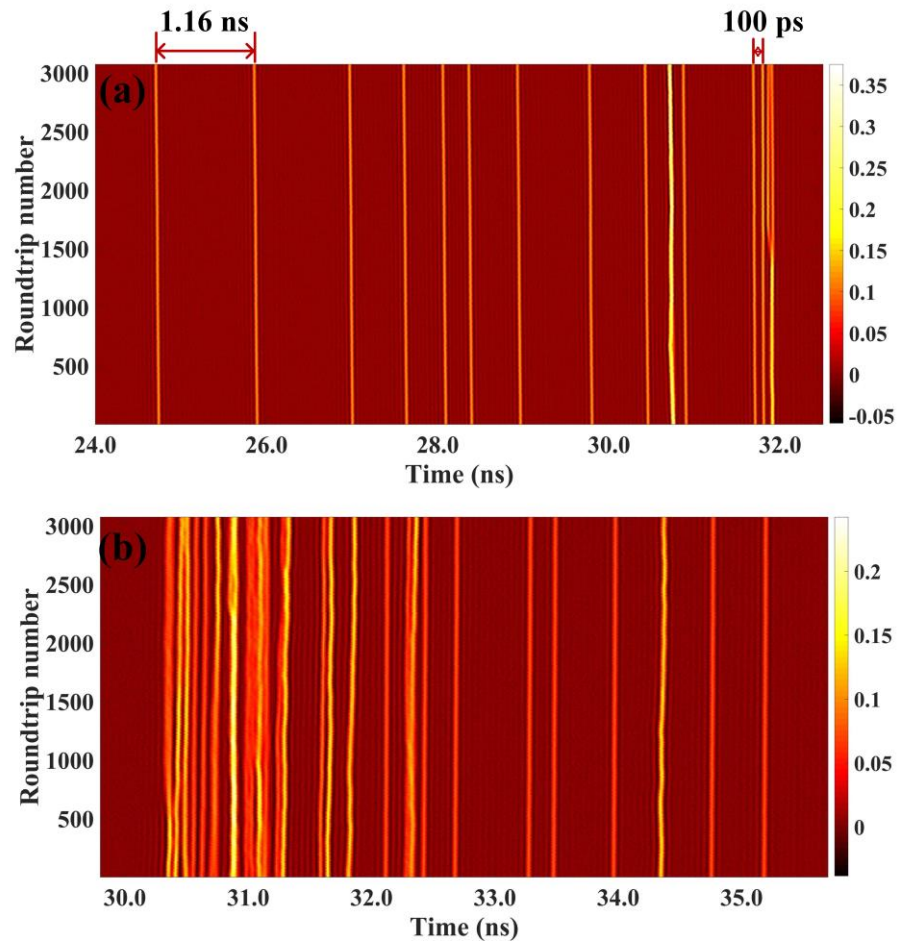


Figure 5. (a) 2D temporal evolution of the pulses with a pump power of 215 mW; (b) 2D temporal evolution of the pulses with a pump power of 415 mW.

In passively mode-locked fiber lasers, the balance of optical dispersion, nonlinearity, gain and loss leads to the generation of soliton pulses. Moreover, due to the peak-power-clamping effect and soliton quantization effect in the anomalous dispersion regime, the soliton pulse can be easily split into multiple pulses. Then, these pulses keep a fixed spacing and constant phase during multiple round trips in the fiber lasers, eventually forming bound solitons, harmonic mode-locked solitons or other special pulse regimes. In our experiment, when the SMS structure was removed from the laser cavity, the mode locking was not observed, indicating that this SMS structure is an indispensable device for the generation of multiple pulses. Thus, a joint result of the nonlinear effect and multimode interference effect of GIME, peak-power-clamping effect and soliton quantization effect at high pump power facilitates the formation of multiple soliton pulses. Additionally, the varying separations in a single multiple-pulse bunch can be associated closely with slow recovery and depletion processes in the fiber laser cavity [49]. Therefore, by appropriately

increasing pump power and finely adjusting PC blades, the unique multiple-pulse operation was achieved in the cavity with the all-fiber SMS device.

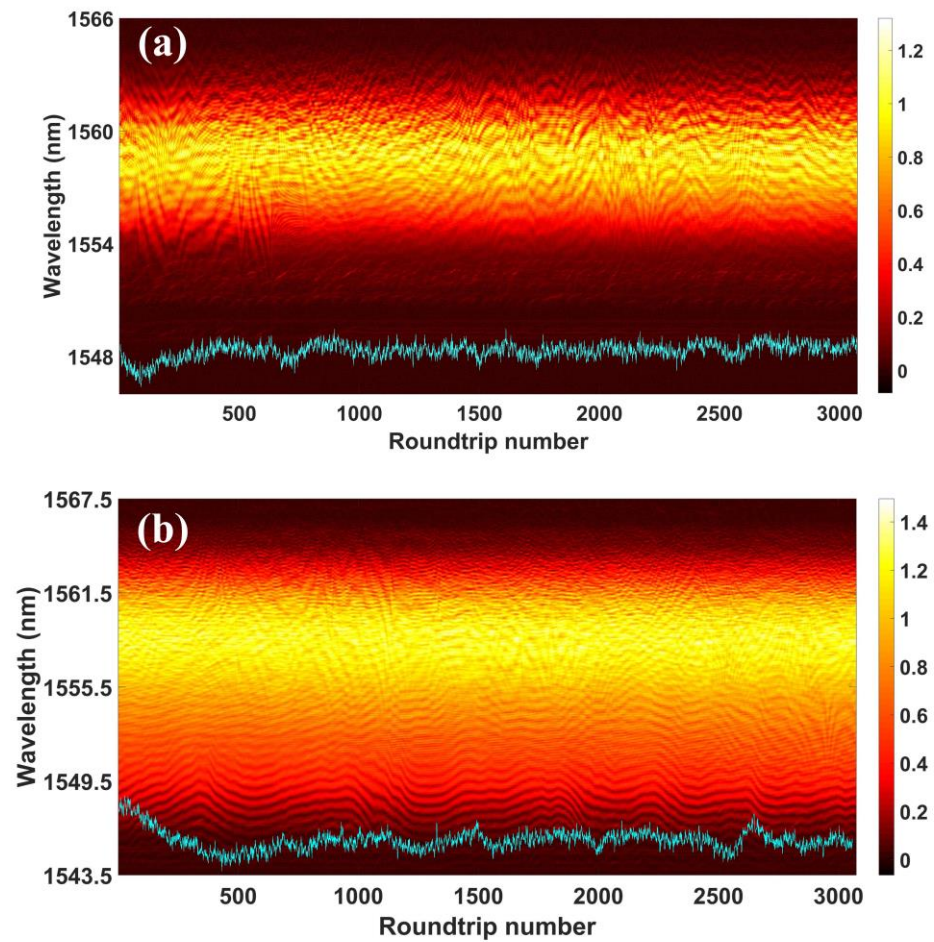


Figure 6. Real-time spectral evolution process. (a) Shot-to-shot spectra at pump power of 215 mW, insert: energy evolution curve; (b) shot-to-shot spectra at pump power of 415 mW, insert: energy evolution curve.

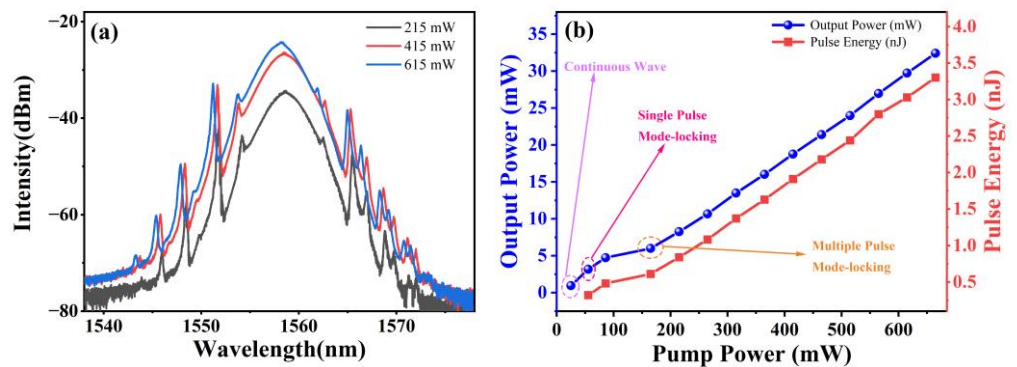


Figure 7. (a) Spectral evolution at different pump powers; (b) operating regime distribution of the laser and the output power and average pulse energy versus the pump powers.

5. Conclusions

In this study, we have reported an erbium-doped fiber laser based on SMS as an excellent SA with a modulation depth of $\sim 8.68\%$, which can generate a stable single pulse and multiple pulses via reorienting the blades of PC and properly changing the pump

power. The single pulse mode-locking state operates at 1558.6 nm with a fundamental repetition rate of 9.84 MHz, and matching SNR up to 58 dB. Moreover, the regime with multiple pulses has average pulse energy from 0.61 nJ to 3.29 nJ with the gradual increase in pump power. Additionally, the dynamic characteristics of multiple pulses are studied by utilizing the DFT technique, indicating that there are randomness and variability in pulse intensities and pulse intervals. These research findings further validate the use of NL-MMI-based SMS as an effective SA in ultrafast fiber lasers.

Author Contributions: Conceptualization, Y.Y. (Yatao Yang) and Q.Z.; methodology, Y.Y. (Yatao Yang), Y.Y. (Yanzhao Yang) and G.D.; writing—original draft preparation and investigation, Y.Y. (Yatao Yang) and Q.Z.; writing, review and editing, J.J. and Y.S.; supervision, Z.W. and K.W.; project administration, Z.W. and K.W. All authors have read and agreed to the published version of the manuscript.

Funding: This study was funded by the National Natural Science Foundation of China (No. 62005178); Natural Science Foundation of Guangdong Province (No. 2023A1515010093); and Shenzhen Fundamental Research Program (Nos. JCYJ20190808112401659, JCYJ20190808143611709, JCYJ20200109105216803 and JCYJ20220809170611004).

Institutional Review Board Statement: Not applicable.

Informed Consent Statement: Not applicable.

Data Availability Statement: Data underlying the results presented in this paper are not publicly available at this time but may be obtained from the authors upon reasonable request.

Conflicts of Interest: The authors declare no conflicts of interest.

References

1. Ebrahim-Zadeh, M.; Sorokina, I.T. *Mid-Infrared Coherent Sources and Applications*; Springer Science & Business Media: Berlin/Heidelberg, Germany, 2008.
2. Ramaswami, R.; Sivarajan, K.; Sasaki, G. *Optical Networks: A Practical Perspective*; Morgan Kaufmann: Cambridge, MA, USA, 2009.
3. Mollenauer, L.F.; Gordon, J.P. *Solitons in Optical Fibers: Fundamentals and Applications*; Elsevier: Amsterdam, The Netherlands, 2006.
4. Mollenauer, L.F.; Mamyshev, P.V. Massive Wavelength-Division Multiplexing with Solitons. *IEEE J. Quantum Electron.* **1998**, *34*, 2089–2102. [[CrossRef](#)]
5. Huang, J.; Yang, S. Investigation on Anisotropic Tribological Properties of Superhydrophobic/Superlipophilic Lead Bronze Surface Textured by Femtosecond Laser. *Appl. Surf. Sci.* **2022**, *579*, 152223. [[CrossRef](#)]
6. Mehta, A.; Mohammed, W.; Johnson, E.G. Multimode Interference-Based Fiber-Optic Displacement Sensor. *IEEE Photonics Technol. Lett.* **2003**, *15*, 1129–1131. [[CrossRef](#)]
7. Goda, K.; Jalali, B. Dispersive Fourier Transformation for Fast Continuous Single-Shot Measurements. *Nat. Photonics* **2013**, *7*, 102–112.
8. Qi, Y.; Yang, S.; Wang, J.; Li, L.; Bai, Z.; Wang, Y.; Lv, Z. Recent Advance of Emerging Low-Dimensional Materials for Vector Soliton Generation in Fiber Lasers. *Mater. Today Phys.* **2022**, *23*, 100622.
9. Chernysheva, M.A.; Krylov, A.A.; Kryukov, P.G.; Arutyunyan, N.R.; Pozharov, A.S.; Obraztsova, E.D.; Dianov, E.M. Thulium-Doped Mode-Locked All-Fiber Laser Based on NALM and Carbon Nanotube Saturable Absorber. *Opt. Express* **2012**, *20*, B124–B130. [[CrossRef](#)]
10. Zhang, M.; Kelleher, E.J.R.; Torrisi, F.; Sun, Z.; Hasan, T.; Popa, D.; Wang, F.; Ferrari, A.C.; Popov, S.V.; Taylor, J.R. Tm-Doped Fiber Laser Mode-Locked by Graphene-Polymer Composite. *Opt. Express* **2012**, *20*, 25077–25084. [[CrossRef](#)] [[PubMed](#)]
11. Xu, Y.; Shi, Z.; Shi, X.; Zhang, K.; Zhang, H. Recent Progress in Black Phosphorus and Black-Phosphorus-Analogue Materials: Properties, Synthesis and Applications. *Nanoscale* **2019**, *11*, 14491–14527.
12. Wu, K.; Guo, C.; Wang, H.; Zhang, X.; Wang, J.; Chen, J. All-Optical Phase Shifter and Switch near 1550nm Using Tungsten Disulfide (WS₂) Deposited Tapered Fiber. *Opt. Express* **2017**, *25*, 17639–17649. [[CrossRef](#)]
13. Yan, P.; Lin, R.; Ruan, S.; Liu, A.; Chen, H.; Zheng, Y.; Chen, S.; Guo, C.; Hu, J. A Practical Topological Insulator Saturable Absorber for Mode-Locked Fiber Laser. *Sci. Rep.* **2015**, *5*, 8690. [[CrossRef](#)]
14. Liu, J.; Xu, J.; Wang, P. High Repetition-Rate Narrow Bandwidth SESAM Mode-Locked Yb-Doped Fiber Lasers. *IEEE Photonics Technol. Lett.* **2012**, *24*, 539–541. [[CrossRef](#)]
15. Yan, P.; Liu, A.; Chen, Y.; Chen, H.; Ruan, S.; Guo, C.; Chen, S.; Li, I.L.; Yang, H.; Hu, J. Microfiber-Based WS₂-Film Saturable Absorber for Ultra-Fast Photonics. *Opt. Mater. Express* **2015**, *5*, 479–489. [[CrossRef](#)]
16. Seredych, M.; Alhabeab, M.; Anasori, B.; Gogotsi, Y. High-Temperature Behaviors of MXenes. In Proceedings of the Electrochemical Society Meeting Abstracts 233; The Electrochemical Society, Inc.: Pennington, NJ, USA, 2018; p. 1136.

17. Nazemosadat, E.; Mafi, A. Nonlinear Multimodal Interference and Saturable Absorption Using a Short Graded-Index Multimode Optical Fiber. *JOSA B* **2013**, *30*, 1357–1367. [[CrossRef](#)]
18. Teğın, U.; Ortaç, B. All-Fiber All-Normal-Dispersion Femtosecond Laser with a Nonlinear Multimodal Interference-Based Saturable Absorber. *Opt. Lett.* **2018**, *43*, 1611–1614. [[CrossRef](#)] [[PubMed](#)]
19. Li, H.; Wang, Z.; Li, C.; Tian, Y.; Xiao, Z.; Zhang, J.; Xu, S. Self-Starting Mode-Locked Tm-Doped Fiber Laser Using a Hybrid Structure of No Core-Graded Index Multimode Fiber as the Saturable Absorber. *Opt. Laser Technol.* **2019**, *113*, 317–321. [[CrossRef](#)]
20. Zhu, T.; Wang, Z.; Wang, D.N.; Yang, F.; Li, L. Observation of Controllable Tightly and Loosely Bound Solitons with an All-Fiber Saturable Absorber. *Photonics Res.* **2019**, *7*, 61–68. [[CrossRef](#)]
21. Jiang, H.; Li, H.; Hu, F.; Ren, X.; Li, C.; Xu, S. Mode-Locked Tm Fiber Laser with a Tapered GIMF SA Based on Nonlinear Multimode Interference Effect. *IEEE Photonics Technol. Lett.* **2020**, *32*, 503–506. [[CrossRef](#)]
22. Li, X.; Wang, D.N.; Chen, J. Saturable Absorber Based on a Hybrid Structure of Graded-Index Multimode Fiber and Graphene for a Passive Mode-Locked Erbium-Doped Fiber Laser. *JOSA B* **2021**, *38*, 2112–2117. [[CrossRef](#)]
23. Zhao, F.; Li, N.; Wang, H. Generation of a Noise-like Pulse from an Erbium-Doped Fiber Laser Based on Nonlinear Multimode Interference. *Laser Phys.* **2020**, *30*, 125102. [[CrossRef](#)]
24. Cheng, P.; Han, M.; Li, Q.; Shu, X. Generation of Different Mode-Locked States in a Yb-Doped Fiber Laser Based on Nonlinear Multimode Interference. *Opt. Express* **2022**, *30*, 35911–35922. [[CrossRef](#)]
25. Ren, X.; Li, H.; Zhang, Z.; Zhang, J.; Xu, S. Generation of Bound Solitons in a Mode-Locked Tm-Doped Fiber Laser Based on a Graded-Index Multimode Fiber Saturable Absorber. *Opt. Laser Technol.* **2022**, *149*, 107865. [[CrossRef](#)]
26. Liu, M.; Qi, Y.; Yang, S.; Bai, Z.; Yan, B.; Ding, J.; Wang, Y.; Lu, Z. Switchable L-Band Dual-Wavelength Dark–Bright Pulse Pair Generation from an Er-Doped Mode-Locked Fiber Laser with SMF–GIMF–SMF as the Saturable Absorber. *Appl. Phys. B* **2022**, *128*, 190. [[CrossRef](#)]
27. Bae, J.E.; Mateos, X.; Aguiló, M.; Díaz, F.; Vázquez de Aldana, J.R.; Romero, C.; Lee, H.; Rotermund, F. Transition of Pulsed Operation from Q-Switching to Continuous-Wave Mode-Locking in a Yb:KLuW Waveguide Laser. *Opt. Express* **2020**, *28*, 18027–18034. [[CrossRef](#)] [[PubMed](#)]
28. Bae, J.E.; Mateos, X.; Aguiló, M.; Díaz, F.; Ajates, J.G.; Romero, C.; Vázquez de Aldana, J.R.; Rotermund, F. Multi-Gigahertz Mode-Locked Femtosecond Yb:KLuW Waveguide Lasers. *Photon. Res.* **2022**, *10*, 2584–2589. [[CrossRef](#)]
29. Bae, J.E.; Calmano, T.; Kränkel, C.; Rotermund, F. Controllable Dynamic Single- and Dual-Channel Graphene Q-Switching in a Beam-Splitter-Type Channel Waveguide Laser. *Laser Photonics Rev.* **2022**, *16*, 2100501. [[CrossRef](#)]
30. Liu, M.; Zhao, N.; Liu, H.; Zheng, X.-W.; Luo, A.-P.; Luo, Z.-C.; Xu, W.-C.; Zhao, C.-J.; Zhang, H.; Wen, S.-C. Dual-Wavelength Harmonically Mode-Locked Fiber Laser with Topological Insulator Saturable Absorber. *IEEE Photonics Technol. Lett.* **2014**, *26*, 983–986. [[CrossRef](#)]
31. Wang, Y.; Mao, D.; Gan, X.; Han, L.; Ma, C.; Xi, T.; Zhang, Y.; Shang, W.; Hua, S.; Zhao, J. Harmonic Mode Locking of Bound-State Solitons Fiber Laser Based on MoS₂ Saturable Absorber. *Opt. Express* **2015**, *23*, 205–210. [[CrossRef](#)]
32. Stratmann, M.; Pagel, T.; Mitschke, F. Experimental Observation of Temporal Soliton Molecules. *Phys. Rev. Lett.* **2005**, *95*, 143902. [[CrossRef](#)]
33. Gattass, R.R.; Cerami, L.R.; Mazur, E. Micromachining of Bulk Glass with Bursts of Femtosecond Laser Pulses at Variable Repetition Rates. *Opt. Express* **2006**, *14*, 5279–5284. [[CrossRef](#)]
34. Seong, N.H.; Kim, D.Y. Experimental Observation of Stable Bound Solitons in a Figure-Eight Fiber Laser. *Opt. Lett.* **2002**, *27*, 1321–1323. [[CrossRef](#)]
35. Allison, S.W.; Gillies, G.T. Observations of and Applications for Self-Imaging in Optical Fibers. *Appl. Opt.* **1994**, *33*, 1802–1805. [[CrossRef](#)] [[PubMed](#)]
36. Agrawal, G.P. Invite Paper: Self-Imaging in Multimode Graded-Index Fibers and Its Impact on the Nonlinear Phenomena. *Opt. Fiber Technol.* **2019**, *50*, 309–316. [[CrossRef](#)]
37. Zhu, X.; Schülzgen, A.; Li, H.; Li, L.; Han, L.; Moloney, J.V.; Peyghambarian, N. Detailed Investigation of Self-Imaging in Largecore Multimode Optical Fibers for Application in Fiber Lasers and Amplifiers. *Opt. Express* **2008**, *16*, 16632–16645. [[CrossRef](#)]
38. Asawa, C.K.; Taylor, H.F. Propagation of Light Trapped within a Set of Lowest-Order Modes of Graded-Index Multimode Fiber Undergoing Bending. *Appl. Opt.* **2000**, *39*, 2029–2037. [[CrossRef](#)] [[PubMed](#)]
39. Su, L.; Chiang, K.S.; Lu, C. Microbend-Induced Mode Coupling in a Graded-Index Multimode Fiber. *Appl. Opt.* **2005**, *44*, 7394–7402. [[CrossRef](#)] [[PubMed](#)]
40. Renninger, W.H.; Wise, F.W. Optical Solitons in Graded-Index Multimode Fibres. *Nat Commun* **2013**, *4*, 1719. [[CrossRef](#)] [[PubMed](#)]
41. Chen, T.; Zhang, Q.; Zhang, Y.; Li, X.; Zhang, H.; Xia, W. All-Fiber Passively Mode-Locked Laser Using Nonlinear Multimode Interference of Step-Index Multimode Fiber. *Photon. Res.* **2018**, *6*, 1033. [[CrossRef](#)]
42. Fu, S.; Sheng, Q.; Zhu, X.; Shi, W.; Yao, J.; Shi, G.; Norwood, R.A.; Peyghambarian, N. Passive Q-Switching of an All-Fiber Laser Induced by the Kerr Effect of Multimode Interference. *Opt. Express* **2015**, *23*, 17255–17262. [[CrossRef](#)]
43. Dong, Z.; Lin, J.; Li, H.; Li, S.; Tao, R.; Gu, C.; Yao, P.; Xu, L. Generation of Mode-Locked Square-Shaped and Chair-like Pulse Based on Reverse Saturable Absorption Effect of Nonlinear Multimode Interference. *Opt. Express* **2019**, *27*, 27610–27617. [[CrossRef](#)]
44. Tang, D.Y.; Zhao, L.M.; Zhao, B.; Liu, A.Q. Mechanism of Multisoliton Formation and Soliton Energy Quantization in Passively Mode-Locked Fiber Lasers. *Phys. Rev. A* **2005**, *72*, 043816. [[CrossRef](#)]

45. Li, C.; Kong, C.; Wong, K.K.Y. High Energy Noise-Like Pulse Generation from a Mode-Locked Thulium-Doped Fiber Laser at 1.7 Mm. *IEEE Photonics J.* **2019**, *11*, 1–6. [[CrossRef](#)]
46. Zhao, Y.; Zhao, D.; Liu, R.; Ma, W.; Wang, T. Switchable Generation of a Sub-200 Fs Dissipative Soliton and a Noise-like Pulse in a Normal-Dispersion Tm-Doped Mode-Locked Fiber Laser. *Appl. Opt.* **2020**, *59*, 3575–3581. [[CrossRef](#)] [[PubMed](#)]
47. Wang, J.; Liang, X.; Hu, G.; Zheng, Z.; Lin, S.; Ouyang, D.; Wu, X.; Yan, P.; Ruan, S.; Sun, Z.; et al. 152 Fs Nanotube-Mode-Locked Thulium-Doped All-Fiber Laser. *Sci. Rep.* **2016**, *6*, 28885. [[CrossRef](#)] [[PubMed](#)]
48. Zhao, L.M.; Tang, D.Y.; Cheng, T.H.; Lu, C. Nanosecond Square Pulse Generation in Fiber Lasers with Normal Dispersion. *Opt. Commun.* **2007**, *272*, 431–434. [[CrossRef](#)]
49. Zaviyalov, A.; Grelu, P.; Lederer, F. Impact of Slow Gain Dynamics on Soliton Molecules in Mode-Locked Fiber Lasers. *Opt. Lett.* **2012**, *37*, 175–177. [[CrossRef](#)]

Disclaimer/Publisher’s Note: The statements, opinions and data contained in all publications are solely those of the individual author(s) and contributor(s) and not of MDPI and/or the editor(s). MDPI and/or the editor(s) disclaim responsibility for any injury to people or property resulting from any ideas, methods, instructions or products referred to in the content.